Activated carbon monoliths from lignocellulosic biomass waste for electrochemical applications

P.O. Ibeh, F.J. García-Mateos, J.M. Rosas, J. Rodríguez-Mirasol, T. Cordero*

Universidad de Málaga, Andalucía Tech, Departamento de Ingeniería Química, Facultad de Ciencias, Campus de Teatinos s/n, 29010 Málaga, Spain

- Corresponding author details

  Phone: 0034952132038

  mail: jmrosas@uma.es

Abstract

The valorization of lignocellulosic biomass waste into bio-based materials is proposed in this work. Cylindrical activated carbon monoliths (ACMs) were prepared from Alcell®, Kraft lignin and olive stone by chemical activation with H_3PO_4. To our best knowledge, there is no previous information about the preparation of ACMs from any type of lignin. The extrusion of the adequate mixing, without any kind of binder, was carried out in an extruder designed by ourselves with different dies. Carbon monoliths without and with holes (25 or 120 channels/cm^2) were obtained. In case of lignin precursors, a stabilization step was optimized to minimize the problems of plasticity and swelling of lignin. N_2 adsorption-desorption at -196 ºC and Hg porosimetry results show that activated carbon monoliths presented pore size distributions in the micro and mesopore range, with high surfaces areas (c.a. 1500 m^2/g) and relatively high mesopore volume (0.35 cm^3/g). The bulk density of the monoliths is also very high (~1.1 g/cm^3 for ACM from Alcell lignin). Electrochemical characterization of binderless activated carbon monolith electrodes was carried out by cyclic voltammetry and galvanic charge-discharge techniques. The ACM from olive stones presents the highest specific capacitance, with approximately 217 F/g.

Keywords: activated carbon monolith; lignin; biomass waste; binderless; phosphoric acid

1. Introduction

The conversion of lignocellulosic biomass waste into bio-based materials can be an interesting route for its valorization, constituting an important incentive for a higher implementation of biorefineries, and a further benefit for biomass waste-generating companies. Among the different possibilities, the preparation of activated carbon from these lignocellulosic biomass waste present many advantages, such as the great versatility and their exponentially increasing demand of these materials. Furthermore, it supposes an opportunity to reduce environmental impacts. In this sense, the structure and composition of lignocellulosic materials make them ideal precursors for the preparation of activated carbons. Activated carbons are usually in form of powder; however, they can be present in different morphologies (powder, pellet, monolith, fiber). The application of the activated carbons will determine the most adequate morphology in each case.

Monolithic configurations usually present large geometric surface area, which results in a low-pressure drop when there are high flow rates, making them very useful materials to be used as adsorbents and supports for catalysts in environmental applications. Activated carbon monoliths (ACMs) have also shown promising results as electrodes for supercapacitors [1-2]. In this sense, the use of ACMs avoids the use of additives, such as binder and conductive agents. Furthermore, the bimodal pore size distribution of ACMs presents the advantage that small pores offer high effective surface area for electrochemical reactions, whereas large pores facilitate electrolyte ingress throughout the structure. In particular, the importance of these macropores is increased when employing an aqueous electrolyte because of the hydrophobic surface of carbon [3]. Additionally, they present relatively higher energy density than powder activated carbons.

Many researchers have come up with different approaches to produce ACMs. They are usually, made by compressing the corresponding activated carbon in the presence of a binder, which usually implies a reduction of pore sizes due to partial blocking, or in less extent in absence of any type of additive by applying a very high pressure [4-8]. Other alternative methods are impregnation of porous ceramic with a carbonaceous solution or simply by the extrusion of an impregnated material with different activating agents, such as H_3PO_4, KOH and $ZnCl_2$, until obtaining the adequate rheological conditions to be extruded [9-16].

There are different methods to prepare activated carbons. In general, activation with phosphoric acid presents several advantages: (a) it occurs in a single or multiple thermal treatment process and leads to a high carbon yield, the acid can be economically recovered, (b) it is effective at relatively moderate temperatures, and (c) it results in materials with mixed porosity that widen the scope of its application.

Specifically, the preparation of binderless ACM from some kind of biomass waste has been already reported. For instance, ACM in form of disks were obtained from coconut shell and African palm by chemical activation with H_3PO_4 solutions [17-19]; ACM with six hexagonal parallel channels were prepared from African palm shells with H_3PO_4, $ZnCl_2$ and $CaCl_2$ solutions [20]; disks from coconut shells with zinc chloride [21]; honeycomb monoliths from orange peel with H_3PO_4, KOH, $ZnCl_2$, and water vapor (neither image was reported in this case) [22]; and pellets from olive stones with H_3PO_4 [23]. These previous works used the activating agent as a binder to proceed with the extrusion, followed by the activation of the ACM. Other methods proposed in the literature prepared disks from fibres of oil palm empty fruit bunches and rubber wood sawdust by direct carbonization, compression and further activation with CO_2, respectively

[2,24]; and disks from olive stones with KOH activation, followed by compression in the presence of polyvinylalcohol as binder [25].

To our best knowledge, there is an important lack of scientific information on the preparation of ACMs from lignin, and only it has been used as raw material for the production of activated carbons [26]. This fact can be associated to the plastic and swelling behavior observed when lignin is pyrolyzed under N_2 atmosphere. Rodriguez-Mirasol et al. noticed a clear relation between the ash content of lignin and the problems above mentioned, observing the disappearance of fusion and swelling when using kraft lignin with ash content above 8% [27]. Nevertheless, this high inorganic percentage in the precursor would lead to a non-desirable high ash content in the final activated carbons.

Therefore, the objective of this work is the preparation of binderless ACMs from lignin and olive stones. The first one derived from the pulp and paper industry and new biorefineries for bioethanol production (from lignocellulosic biomass); and the second one obtained in the olive industry. Kraft and Alcell® lignin, and olive stones, impregnated with H_3PO_4, are extruded, and subsequently activated. The obtention of disks and monoliths with different amount of channels are also evaluated. In order to minimize the possible fusion and swelling of lignin during activation, different approaches have been tested. Furthermore, the electrochemical properties of the ACMs are analyzed.

2. Experimental

2.1. ACM preparation

The ACMs were prepared from different biomassic precursors: Alcell® lignin (AL) (Repap Technologies Inc.); eucalyptus Kraft lignin (KL); and olive stone (OS) supplied by S.C.A.

Olivarera and Frutera San Isidro, Periana (Málaga). The raw materials were milled and sieved to particle size range of 50-80 μm.

These precursors were impregnated with H_3PO_4 in an impregnation ratio of 1 (H_3PO_4/raw material), and kept in a vacuum dryer for 24 hours, at 60 ºC. In order to study the effect of the impregnation ratio, olive stone was also impregnated with an impregnation ratio of 2. The dried impregnated samples were mixed with distilled water to obtain the adequate rheological properties and plasticity to permit their extrusion. Therefore, the impregnated samples, without any kind of binder, were extruded in a extruder designed by our research group, using a cylindrical mould with an internal diameter of 2 cm, at room temperature and 0.8 MPa. The extruder is composed of different high quality designed die elements (internal diameter of 1 cm), with the aim of obtaining different type of monoliths (compact disc; 25 and 120 channels/cm^2; respectively). When both lignins were used as raw materials, a stabilization step of the impregnated samples, previous to the extrusion, was necessary to partially avoid the swelling problems. The optimized methods consists of a thermal treatment at 250 ºC, under air flow (150 cm^3/min), for 1 h. Then, 50% of the stabilized material was milled and mixed with 50 % of non-stabilized impregnated lignin, obtaining a paste that finally is extruded to form the monoliths.

Subsequently, the obtained monoliths were activated in a tubular furnace at 700 ºC for 2 h, with a heating rate of 10 ºC/min. Finally, activated monoliths were washed with distilled water at 60 ºC, until constant pH in the eluate.

2.2. Characterization

Ultimate analysis of the samples was performed using a LECO CHNS 932 system, and the corresponding oxygen content was calculated by difference. The ash content of the ACMs was calculated from the weight of the solid residue after being gasified in air at 900 ºC.

The porous texture of the ACMs was evaluated by N_2 adsorption–desorption at -196 ºC and CO_2 adsorption at 0 ºC, using a micrometrics instrument (ASAP 2020 model) and by Hg porosimetry (Autopore IV model). The ACMs were previously outgassed for 8 h at 150 ºC. The corresponding textural parameters were calculated by applying the BET equation and the t-method from the N_2 isotherm data; and the Dubinin–Radushkevich equation from the CO_2 adsorption data.

Surface chemistry of the ACMs was analyzed by temperature-programmed desorption (TPD). CO and CO_2 profiles were obtained in a custom quartz fixed bed reactor placed inside an electrical furnace and quantified by non-dispersive infrared (NDIR) gas analyzers (Siemens ULTRAMAT 22). The samples were heated from room temperature to 930 ºC at a heating rate of 10 ºC/min in N_2 flow.

The real density of the ACMs was measured by helium pycnometer using an AccuPyc II 1340 equipment. The surface texture and structure of the ACMs were characterized by scanning electron microscopy (SEM), with a JEOL JSM-6490LV instrument, obtained at a high voltage of 20–25 kV.

The electrochemical performance was studied by using a standard three electrode cell comprising of a platinum wire as counter electrode, Ag/AgCl electrode as reference electrode and a working electrode that contains the corresponding ACM, which was cut (thickness= 200 μm) and dried at

100ºC in a vacuum oven. Counter collector consists of a stainless steel mesh. Working and counter electrodes were placed face-to-face and tested in 1 M H_2SO_4 electrolyte. Samples were characterized by cyclic voltammetry technique at a scan rate of 1 mV s^{-1} in an electrochemical analyzer, model SP-200 (Bio-Logic Int.).

3. Results and discussion

Figure 1 shows a representation of the extruder designed by our research group for the preparation of the ACMs. The extruder consists mainly of a cylindrical mould of stainless steel with an internal diameter of 2 cm, and different die elements (internal diameter of 1 cm), operated at room temperature. The set-up is able to provide a maximum of 1.6 MPa, although in the preparation of these ACMs, the pressure has not exceeded, in any case 0.8 MPa. Two different die elements were also designed with 19 and 72 pins to obtain monoliths with 25 and 120 channels/cm^2, respectively.

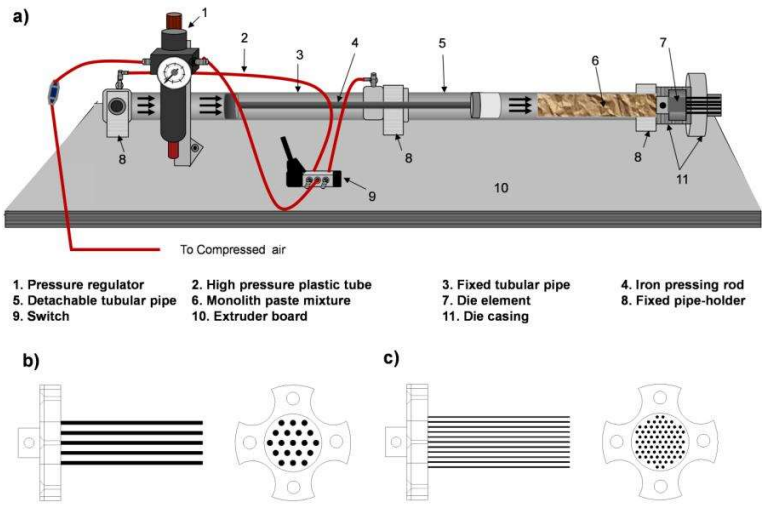

Figure 1. Components of the home-made extruder designed for the ACM preparation.

Table 1 summarizes the ash content and ultimate analysis of the different raw materials. KL presents a high ash content, about 12.4 %, in contrast to AL and OS with very low proportions. AL shows the highest percentage of carbon content (about 65 %). Furthermore, no trace of sulphur is observed in samples AL and OS. In the case of KL, the significant S (%) is derived from its preparation procedure (Kraft pulping or sulfate process).

Table 1. Ash content and ultimate analysis of the different precursors in dry ash free (daf).

Precursor	**Ash (%)**	**C (%)**	**H (%)**	**N (%)**	**S (%)**	**O (%)***
OS	0.4	48.04	7.32	0.30	n.d.	44.34
AL	0.1	64.80	6.30	0.20	n.d.	28.70
KL	12.4	58.22	6.28	0.11	1.83	33.56

*by difference

The circular shaped monoliths obtained before the activation step present a cross section with a diameter of 0.9 cm. **Figure 2** shows some SEM micrographs of the different types of ACMs prepared from AL. As can be seen, the configuration of the extruder allows for obtaining disks and monoliths with 25 and 120 channels/cm^2 at very low pressure (0.8 MPa) compared to those reported in the literature obtained at 130 MPa [28-29]. ACMs undergo shrinkage of their sizes after the activation step. For instance, the diameter of the cross sectional view in the monoliths OS and AL at the same impregnation ratio, are reduced to approximately 25%. In general, the density cell of the different ACMs varies from 30 to 125 cell/cm^2, the wall thickness was from

250 to 800 μm, the hydraulic diameter was from 0.7 to 4 cm, the open frontal area was between 5 and 25 %, and the geometric surface area varies from 0.7 to 1 cm^2/cm^3. **Figure 3** represents some SEM micrographs of the ACMs disks for the different raw materials: OS, AL, KL. It is important to mention that the ACMs obtained from lignin needed a previous stabilization treatment to avoid swelling during the activation step. As can be seen, OS and AL monoliths appeared to be very similar. In contrast, Kraft lignin monolith shows more similar xerogel-like morphology as shown in Fig. 3(c).

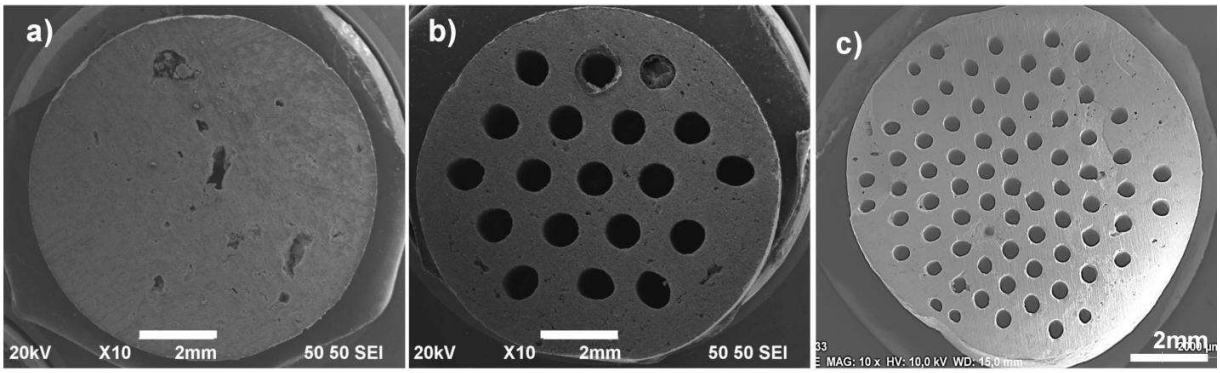

Figure 2. SEM micrographs of the activated carbon monoliths a) carbon disk; b) monolith with 25 channels/cm^2; c) monolith with 120 channels/cm^2.

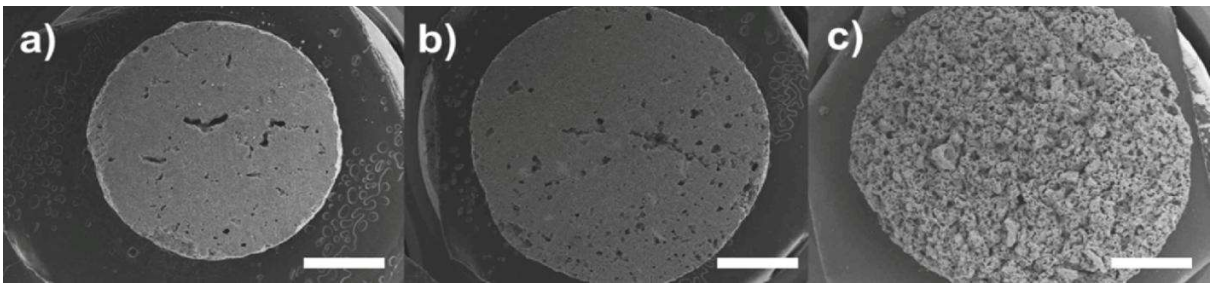

Figure 3. SEM micrographs of the activated carbon monoliths disks from OS1; AL1; and KL1, respectively. Bar length: 2 mm.

Table 2 shows the yields and ultimate analyses of the ACMs. Yield is related to the composition of the raw material, i.e. hemicellulose, cellulose and lignin content. The highly aromatic and carbon-rich molecular structure of lignin devolatilizes to a lesser extent than cellulose and hemicelluloses [30]. In this sense, olive stones contain approximately 26–32% of lignin [31], which explains the lower yield of this monolith compared to that of Alcell lignin. In the case of Kraft lignin, the high ash content of this precursor is a probable explanation of its yield, which can be also directly related to the lowest carbon content obtained by the ultimate analysis. On the other hand, yields of OS, AL and KL monoliths are similar to those reported for different AC by Yakout et al., from OS [32]; Rosas et al., from AL [33], and Montane et al., from KL [34] respectively. Although these last ACs were obtained at different impregnation ratios. As expected, the yield of OS monoliths decreases with the impregnation ratio, as a consequence of a deeper dehydration of the carbonaceous structure of the precursor [35], and the corresponding carbon content increases [36-37]. These results suggest that the conformation into monoliths does not produce any significant influence of the yields of the obtained ACMs.

Table 2. Yields and ultimate analyses of the ACMs in dry ash free (daf).

Monoliths	Yield (%)	C (%)	H (%)	N (%)	S (%)	O (%)*
OS1	39.5	78.96	3.73	0.31	n.d.	16.99
OS2	28.8	81.72	3.26	0.42	n.d.	14.60
AL1	40.5	86.26	3.95	0.31	n.d.	9.47
KL1	32.0	78.22	3.47	0.22	0.98	17.12

*by difference, includes P content.

Figure 4 represents the N_2 adsorption-desorption isotherms of the ACMs disks at -196 ºC. It is important to mention that no significant differences were found in the N_2 adsorption-desorption isotherms of the different type of monoliths (disks; 25 and 120 channels/cm^2) from the same precursor. ACMs obtained from both Kraft and Alcell lignin show type I isotherms characteristic of typical microporous solids, where almost all N_2 volume adsorbed takes place at low relative pressures. Specifically, Kraft lignin-derived monolith presents a more pronounced horizontal plateau, starting at very low relative pressure, indicating the presence of narrower microporosity. The monoliths obtained from olive stone show a type IV isotherm with an increase of the adsorbed volume in the entire relative pressure range, in general, the sample obtained at higher impregnation ratio presents a large amount of porosity with microporous and mesoporous structures. As it is well known, the increase of the relative amount of activation agent generates a higher development of porosity, widening the porous structure of the monoliths [38].

On the other hand, the porosity development of the ACMs, at the same impregnation ratio, follows the sequence: OS>AL>KL, probably due to the presence of cellulose in OS. In this line, Guo and Rockstraw pointed out the great influence of the precursor in the porosity development, showing higher surface areas in carbons obtained from cellulose than those from Kraft lignin, at impregnation ratios equal or higher than 1 [39].

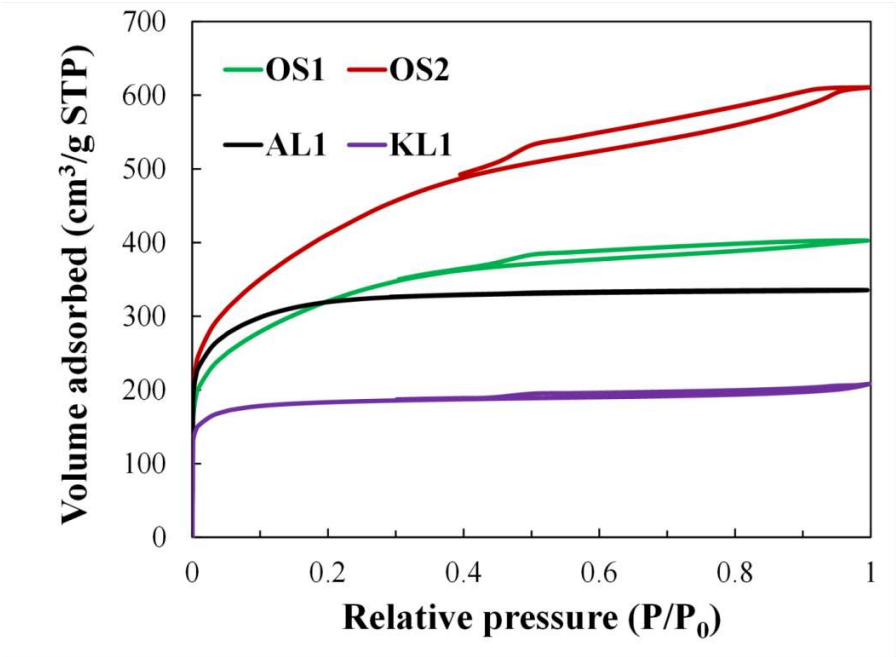

Figure 4. N_2 adsorption-desorption isotherms of the ACMs disks at -196 ºC.

Figure 5 shows the pore size distribution (PSD) of the ACMs derived from both the N_2 adsorption-desorption at -196 ºC and Hg porosimetry. With regard to the macroporosity, shown in the right side of the figure, the features observed in SEM micrographs are corroborated in the PSD, and the monolith from kraft lignin exhibits the highest contribution of macroporosity. In contrast, the presence of macropores in monoliths from olive stone is lower than that in monoliths from lignin. The left side of the figure shows the PSD obtained from N_2 adsorption-desorption at -196 ºC. A broad pore size distribution was observed in all cases. All the ACMs present a predominant peak center around 0.7 nm and a second peak at pore sizes between 1.4 and 2.0 nm. The monoliths prepared from Kraft and Alcell lignin show a bimodal distribution in the micropore range. In the case of ACMs prepared from olive stone (OS1 and OS2), a wider pore size distribution is observed, obtaining mesopores up to 4 nm. This effect is more noticeable

in the sample OS2 due to the higher impregnation ratio, which produces a broadening of the porosity.

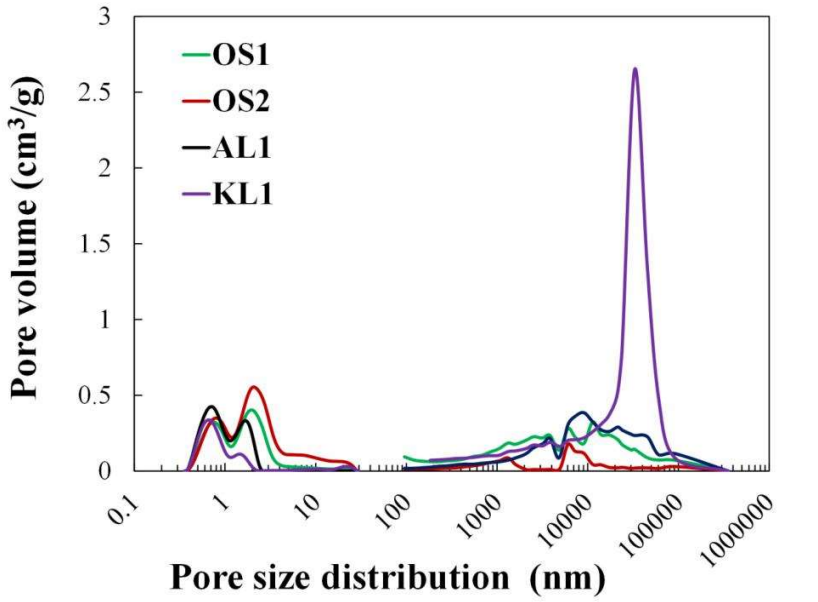

Figure 5. Pore size distribution (PSD) of the ACMs disks derived from both the N_2 adsorption-desorption at -196 ºC and Hg porosimetry.

Table 3 summarizes the textural parameters of the ACMs. The porosity percentage and the true density were also collected in this table. The monoliths exhibit apparent surface areas (A_{BET}) between, 700 to 1500 m^2/g, which indicate the well-developed porous structure produced after the activation step. ACMs prepared from lignin (AL1 and KL1) present lower values of external area (A_t) and mesopore volume (V_{mes}). On the other hand, when olive stone is used as precursor, higher external surface area and mesopore volume are observed, obtaining at the impregnation ratio of 2, A_t=300 m^2/g and V_{mes}=0.35 cm^3/g. Micropore volumes derived from CO_2 adsorption at 0 ºC are quite similar in all monoliths, ranging around 0.25 cm^3/g. For the sake of comparison, activated carbons obtained at the same experimental conditions than those used for monoliths

were also prepared. The analysis of the porosity suggests that the extrusion does not modify substantially the porous structure of the activated carbon, even in some cases, a slight increase of the apparent surface area was observed.

As aforementioned, there is certain lack of knowledge about the preparation of ACM from lignin. However, there are some works related to the obtention of ACM from olive stones. In this sense, the values of the apparent surfaces area are higher than some pellets reported in the literature [23], and the micropore volumes are in the same order than others [15]. In any case, the possibility of obtaining monoliths not only with higher porosity development, but also with different amount of channels, is an additional advantage compared to pellets, since the pressure drop associated to some applications, such as like adsorbents or catalysts, could make these ACMs into quite attractive materials. Specifically in electrochemical applications, the contact between particles in monoliths is much better than that observed in pellets made from compaction under pressure of a powdered carbon [40].

The density of monoliths is also of great interest, overall, in the gas storage applications, where adsorption on a volumetric basis is an important design parameter [41]. The true density of the monoliths is around 1.75 g/cm^3, but an increase of this value can be observed from OS to KL, at the same impregnation ratio. The true density of OS also increases with the impregnation ratio, as a consequence of the dehydration reaction at low temperature that would facilitate further repolimerization and condensation reaction and conversion to carbon [15]. The values obtained from the different precursors are quite similar to those reported in the literature from different lignocellulosic precursors [15,28]. It is important to point out that the monolith (from Kraft lignin) with higher true density also shows the highest porosity percentage, 64%. A relevant

parameter in electrochemical applications is the bulk density, which can be calculated from the porosity and the true density. The values here obtained are ranging from 0.7 for KL1 to 1.4 g /cm^3 for OS1, these values are considerably higher than others reported in the literature with monoliths obtained by compression of a powdered carbon [42-43].

Table 3. Physico-chemical parameters of the ACMs.

Sample	N_2 adsorption				CO_2 adsorption				TPD	
	A_{BET} (m^2/g)	Vt (cm^3/g)	A_t (m^2/g)	V_{mes} (cm^3/g)	A_{DR} (m^2/g)	V_{DR} (cm^3/g)	Ø (%)	ρ_{Tavg}^{He} (g/cm^3)	CO (mmol/g)	CO_2 (mmol/g)
OS1	1147	0.50	115	0.12	622	0.25	17.5	1.69	4.2	0.6
OS2	1489	0.59	297	0.35	638	0.26	48.0	1.82	6.4	0.4
AL1	1054	0.49	29	0.02	734	0.29	38.9	1.77	6.1	0.5
KL1	682	0.28	23	0.09	569	0.23	63.8	1.85	9.5	0.7

Figure 6 shows the CO (a) and CO_2 (b) evolution from TPD analyses of the different ACMs. The activated carbon monoliths show most of the CO evolution at high temperatures, which can be attributed to the presence of C-O-PO_3 groups formed during the activation of phosphoric acid, as reported by our research group in previous studies [33,44]. Wu and Radovic also reported the formation of this kind of groups by impregnating carbon/carbon composite samples with a methanol solution of methyl-phosphoric acid or phosphorus oxychloride and heating at ca. 600 ºC [45]. A lower amount of CO is desorbed at temperatures below 700 ºC, due to decomposition of anhydride, phenol and ether groups. The amount of CO_2 evolved (Fig. 6.b) from the ACMs is significantly lower than that corresponding to CO evolution, indicating a lower concentration of

carboxyl, lactonic and anhydride surface groups. The monolith with the highest presence of CO-evolving groups is that from Kraft lignin. This feature is quite relevant, because the surface oxygen groups that decompose as CO are reported to be more electrochemically active than CO_2-evolving groups, which can actively contribute to charge storage by pseudocapacitive reactions [46]. The total amounts of CO and CO_2 released during the TPD analyses are also summarized in Table 3. As can be seen, the amounts of CO desorbed are significantly higher for the sample KL1, and very similar for the AL1 and OS2 carbon monoliths.

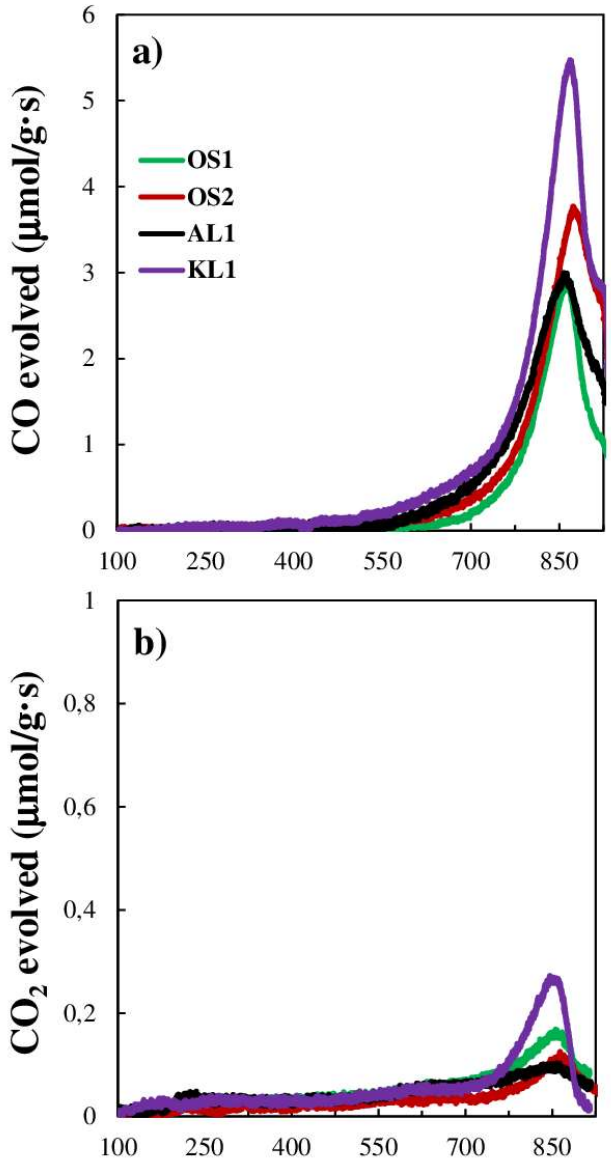

Figure 6. CO (a) and CO_2 (b) evolution during the TPD of the different ACMs disks.

ACMs disks were tested in a three electrode cell with H_2SO_4 as electrolyte to evaluate their electrochemical performance. Cyclic voltammetries were carried out for the potential window from 0 to 0.8 V, at a scan rate of 1 mV/s. Figure 7.a shows the cyclic voltammograms of ACMs and 7.b the corresponding galvanostatic charge-discharge curves. ACM electrode from OS2

exhibits the highest current responses at this scan rate, followed by the KL1, AL1 and OS1 monolith. Based on the mechanism of double-layer charge/discharge, the specific capacitance of the ACMs should be directly proportional to their apparent surface area (A_{BET}) [47]. In that case, OS2 also presents the highest surface area and pore volume. However, KL1 shows a remarkable electrochemical performance in spite of its low surface area and pore volume. This anomalous result suggests that the specific capacitance of the ACMs was not only contributed by the double-layer charge/discharge at the electrode–electrolyte interface but also by the redox transitions of surface functional groups (i.e., pseudo-capacitance) [48] and/or by the differences of the starting material [49]. In this sense, KL1 presents the highest amount of surface functional groups, which desorb as CO during TPD (as reported in Table 3).

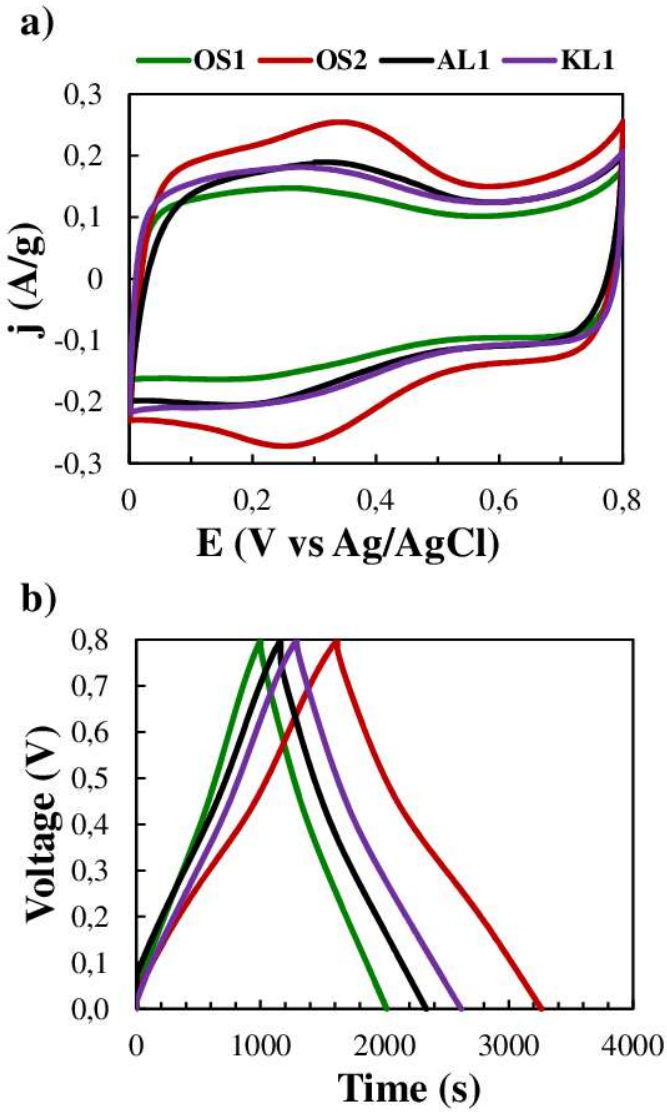

Figure7.(a) Voltammogram data obtained at 1 $mV \cdot s^{-1}$; (b) Galvanostatic charge-discharge curves for the different ACMs disks.

The constant current charge-discharge studies of the supercapacitor cell were performed between cell voltages of 0.01 and 0.8 V, at a discharge current density of 50 mA/g. The shape of the

charge–discharge curves are closely linear and show a typical symmetric triangular distribution, indicating a good double layer capacitive property. Comparative values of specific capacitance from galvanostatic charge-discharge and cyclic voltammetry are listed in Table 4 for all the ACMs electrodes. The different methods to calculate specific capacitances reveal the same tendency. There is not a clear relationship between the specific capacitance values and the apparent surface area, suggesting the great influence of the type of precursor and the pseudo-capacitance. The values of capacitances for the ACMs are comparable or even better than others reported in the literature, with similar porosity [50], but the advantage of these materials is the use of a simple preparation method to obtain ACM electrodes from biomass waste precursors.

Table 4. Specific capacitances obtained from cyclic voltammetry (CV) and constant current charge-discharge (GCD) methods of the ACMs electrodes.

Electrodes	**C_g^{CV} (F/g)**	**C_g^{GCD} (F/g)**
OS1	122	134
OS2	191	217
AL1	144	161
KL1	151	166

Conclusions

A series of cylindrical activated carbon monoliths (ACMs) were prepared by chemical activation of different lignocellulosic biomass waste such as olive stone, Alcell and kraft lignin with

phosphoric acid at different impregnation ratios. To our best knowledge, there is no previous information about the preparation of ACMs from any type of lignin. The extrusion of the adequate mixing, without any kind of binder, was carried out in a home-made extruder with different die elements. This method allows for obtaining disks and monoliths with 25 and 120 channels/cm^2.

In the case of lignin precursors, a stabilization step becomes necessary to minimize the problems of plasticity and swelling. Half of the impregnated sample is treated at 250 ºC in air and mixed to the rest of impregnated sample before the extrusion. This method is valid for Alcell lignin. In the case of Kraft lignin, a partial contraction of the size is noticed. An activated micropore carbon monolith with an apparent surface area of about 1500 m^2/g, with micropore volume of 0.538 cm^3/g was obtained at 700 ºC with an impregnation ratio of 2, using olive stone as precursor. The bulk density of the monoliths is also very high (~1.1 g/cm^3 for ACM from Alcell lignin). This high density opens the whole range of possibilities for different applications.

Electrochemical characterization was carried out by cyclic voltammetry and galvanic charge-discharge techniques with electrodes from ACMs in the absence of any type of binder and conductivity promoter. The olive stone monolith presents the highest specific capacitance of all the ACMs, approximately 217 F/g. This value is higher than others reported in the literature for activated carbons obtained from lignocellulosic precursors.

Acknowledgements

This work was supported by the Spanish Ministry of Economy and Competitiveness through CTQ2015-68654-R project.

References

[1] V. Ruiz, C. Blanco, R. Santamaría, J.M. Ramos-Fernández, M. Martínez-Escandell, A. Sepúlveda-Escribano, F. Rodríguez-Reinoso. An activated carbon monolith as an electrode material for supercapacitors. Carbon 47 (2009) 195 –200.

[2] N. S. M. Nor, M. Deraman, R. Omar, E. Taer, Awitdrus, R. Farma, N. H. Basri, and B. N. M. Dolah. Nanoporous separators for supercapacitor using activated carbon monolith electrode from oil palm empty fruit bunches. AIP Conference Proceedings 68 (2014) 1586.

[3] G. Hasegawa, K. Kanamori, T. Kiyomura, H. Kurata, T. Abe. K. Nakanishi. Hierarchically Porous Carbon Monoliths Comprising Ordered Mesoporous Nanorod Assemblies for High-Voltage Aqueous Supercapacitors. Chem. Mater 28 (2016) 3944-3950.

[4] D. Lozano-Castelló, D. Cazorla-Amorós, A Linares-Solano, D.F. Quinn. Activated carbon monoliths for methane storage: influence of binder. Carbon 40 (15) (2002) 2817-2825.

[5] J.-W. Lim, Y. Choi, H.-S. Yoon, Y.-K. Park, J.-H. Yim, J.-K. Jeon. Extrusion of honeycomb monoliths employed with activated carbon-LDPE hybrid materials. Journal of Industrial and Engineering Chemistry 16 (2010) 51-56.

[6] V. Solís, L. Liu, Z. Liu, Z. Huang, P. Liu. Preparation of activated honeycomb monoliths. Carbon 45 (2007) 2836-2842.

[7] J. Machnikowski, K. Kierzek, K. Lis, H. Machnikowska, L. Czepirski. Tailoring Porosity Development in Monolithic Adsorbents Made of KOH-Activated Pitch Coke and Furfuryl Alcohol Binder for Methane Storage. Energy & Fuels 24 (2010) 3410-3414.

[8] M. J. Beneyto, D. L. Castelló , F. S. García, D. C. Amorós, Á. L. Solano. Advanced activated carbon monoliths and activated carbons for hydrogen storage. Microporous and Mesoporous Materials 112 (2008) 235–242.

[9] E. Garcia-Bordeje, F. Kapteijn, J.A. Moulijn, Preparation and characterization of carbon-coated monoliths for catalyst supports. Carbon 40 (2002) 1079-1088.

[10] J. Ozaki, N. Endo, W. Ohizumi, K. Igarashi, M. Nakahara, A. Oya, S. Yoshida, T. Iizuka . Novel preparation method for the production of mesoporous carbon fiber from a polymer blend. Carbon 35 (1997) 1031-1033.

[11] F. S. Lazar, T. Chaieb, S. Pallier, L. Veyre, R. Philippe, V. Meille. Direct coating of carbon-supported catalysts on monoliths and foams -Singular behaviour of Pd/MWCNT. Applied Catalysis A: General 508 (2015) 45–51.

[12] E. Lam, J. H.T. Luong. Carbon Materials as Catalyst Supports and Catalysts in the Transformation of Biomass to Fuels and Chemicals. ACS Catalysis 4 (2014) 3393-3410.

[13] D. Hulicova, A. Oya. The polymer blend technique as a method for designing fine carbon materials. Carbon 41 (7) (2003) 1443-1450.

[14] T. Vergunst, M.J.G. Linders, F. Kapteijn, J.A. Moulijn. Carbon-based monolithic structures. Catal. Rev.-Sci. Eng. 43 (2001) 291-314.

[15] M.M. Sabio, C. Almansa, F.Rodriguez-Reinoso. Phosphoric acid activated carbon disks for methane adsorption, Carbon 41 (2003) 2113-2119.

[16] A.F. Pérez-Cadenas, F. Kapteijn, J.A. Moulijn, F.J. Maldonado-Hódar. Pd and Pt catalysts supported on carbon-coated monoliths for low-temperature combustion of xylenes. Carbon 44 (2006) 2463-2468.

[17] D.P. Vargas, L. Giraldo, J. Silvestre-Albero, J.C. Moreno-Piraján. CO_2 adsorption on binderless activated carbon monoliths. Adsorption 17 (2011) 497-504.

[18] D. D. P. Vargas, G. L. Giraldo, P. J. C. Moreno. Enthalpic characterisation of activated carbon monoliths obtained from lignocellulosic materials. J Therm. Anal. Calorim 111 (2013) 1067–1072.

[19] J.C.A. de Oliveira, R. B. Rios, R.H. López, G. Zgrablic. Monte Carlo Simulation Strategies for Predicting CO2 /CH4 Adsorption onto Activated Carbons from Pure Gas Isotherms. Adsorption Science and Technology 29 (2011) 651-661.

[20] D.P. Vargas, L. Giraldo, J.C. Moreno-Piraján. CO_2 Adsorption on Activated Carbon Honeycomb-Monoliths: A Comparison of Langmuir and Tóth Models. Int. J. Mol. Sci. 13 (2012) 8388-8397.

[21] A.A. G. Blanco, J.C. A. de Oliveira, R. López, J.C. M. Piraján, L. Giraldo, G. Zgrablich, K. Sapag. A study of the pore size distribution for activated carbon monoliths and their relationship with the storage of methane and hydrogen. Colloids and Surfaces A: Physicochem. Eng. Aspects 357 (2010) 74–83.